ELSEVIER

Journal of Nuclear Materials 265 (1999) 139–145

journal of nuclear materials

Helium implanted *Zr*Hf as studied by time differential perturbed angular correlation and positron lifetime measurements

R. Govindaraj [a,*], G.Venugopal Rao [a], K.P. Gopinathan [b], B. Viswanathan [a]

[a] *Metal Physics Laboratory, Materials Science Division, Indira Gandhi Centre for Atomic Research, Kalpakkam 603 102, India*
[b] *Department of Physics, Cochin University of Science and Technology, Cochin 682 022, India*

Received 21 May 1998; accepted 24 August 1998

Abstract

Time differential perturbed angular correlation (TDPAC) at the 482 keV state of ^{181}Ta and positron lifetime measurements were performed on homogeneously helium implanted *Zr*Hf samples. TDPAC on the as-implanted sample shows the association of 0.12 ± 0.02 fraction of probe nuclei with stacking faults experiencing a local fcc environment. The dissociation of this defect complex from probe nuclei is observed following the annealing treatment at 423 K. TDPAC measurements lead to the conclusion that Hf impurities do not bind He-vacancy complexes or helium bubbles in *Zr*Hf. A recovery stage associated with helium migration is identified from the variation of the relative width of the Lorentzian distribution of the quadrupole frequency in TDPAC measurements. This correlates well with the variation of the helium associated positron lifetime component. The nucleation and growth stages of He bubbles in the sample have been identified by positron lifetime measurements as a function of the annealing temperature on the irradiated sample. Based on the analysis of positron lifetime measurements, helium bubble parameters such as bubble radius and bubble concentration have been extracted in the growth stage, leading to a quantitative understanding of the bubble growth in *Zr*Hf.

1. Introduction

In recent years considerable effort has been directed towards the study of the behaviour of helium in metals, as helium is produced by (n, α) nuclear reactions in nuclear materials. Helium atoms are insoluble in metals and are strongly attracted by vacancies. Implantation of α-particles in metals leads to the formation of He–V complexes and helium stabilised vacancy clusters [1,2]. In post-irradiation annealing studies re-arrangement of He–V complexes leading to the nucleation and growth of helium bubbles have been reported [3]. As helium atoms are strongly bound to open volume defects an attractive interaction between the latter and impurities present in a sample would lead to the formation of He–V-impurity complexes [4]. Therefore, depending upon the interaction of the impurity with the vacancy there would either be an acceleration [5] or deceleration [6] of growth of He bubbles.

The hyperfine interaction of such impurities, meaning the interaction between the nuclear moments of impurities and electromagnetic field at their sites in a sample [7], provides a powerful method for studying defects associated with probe nuclei. This is based on the principle that probe nuclei associated with a defect experience unique magnetic field and/or electric field gradient different from that of the probe nuclei which are defect free and substitutional in the sample. The hyperfine interaction induced perturbation of angular correlation of γ rays emitted in cascade by suitable radioactive probe atoms introduced in the sample (TDPAC), has been established as a powerful technique for studying defects in solids [8,9]. These techniques such as TDPAC, Mossbauer spectroscopy etc., have been extensively used in studying the behaviour of helium in metals [10].

* Corresponding author. E-mail: rgovind@igcar.ernet.in

0022-3115/99/$ – see front matter
PII: S0022-3115(98)00513-3

Positron annihilation spectroscopy [11] is a powerful technique for studying small vacancy clusters. As the positron lifetime [11,12] is sensitive to open volume defects in the sample, it is extensively used in the study of inert gas decoration of vacancy clusters [13]. Positron lifetime shows a sensitive dependence upon the helium to vacancy ratio in vacancy clusters of radius <0.5 nm [13]. Thus the defect specificity of PAS, combined with the sensitivity to helium decoration, could be effectively used for a quantitative and qualitative understanding of properties of helium bubbles over a wide size range. There has been a lot of studies on helium in metals by positron annihilation spectroscopic techniques leading to a detailed understanding of nucleation and growth of bubbles [14].

Zr metal and its alloys are used for the cladding of thermal reactor fuel materials for calendria and pressure tubes in CANDU reactors. The presence of impurities in Zr metal significantly alters the defect recovery stages. The effect of various solute-defect interaction in α-Zr has been discussed by Hood [15]. Hf is inevitably present in dilute concentration in Zr metal. The chemical properties and ionic radii of Zr and Hf are similar and their valences are the same. It is of technological interest to know whether Hf impurities bind helium implantation induced defects and thereby play any critical role in controlling the helium bubble growth in α-Zr.

The sample *Zr*Hf being hcp and non-magnetic, the hyperfine interaction as experienced by Hf impurities would essentially be between the nuclear quadrupole moment of the Hf nuclei at the isomeric state of interest and electric field gradient (EFG) at their sites in the sample. The change of microscopic structure of the lattice due to a defect produces changes in the local electron density distribution which can result in changes in EFG at Hf impurities in α-Zr matrix. The EFG at a probe atom due to the presence of a defect in the sample varies inversely as the cube of the distance between them. Therefore the defects which are trapped by probe nuclei alone are visible in the experiment. The measurement of hyperfine interaction parameters of probe nuclei such as the asymmetry of the charge distribution at their sites and various fractions of probe nuclei experiencing unique EFGs would lead to an identification of defects simultaneously occurring in the sample. This is possible when the hyperfine interaction parameters are correlated with the mode of defect production, and other experimental results such as resistivity recovery studies etc. A study of the variation of the fractions of probe nuclei with isochronal annealing treatment of the sample would lead to an understanding of the mobility of defects and their clustering.

TDPAC and positron lifetime measurements could be used as complimentary techniques in studying defects in materials. By the former only defects that are trapped by (associated with) probe atoms could be detected, which is determined by the nature of the interaction (attractive or repulsive) between the defect and impurity. The stability of the probe-defect complex is dictated by its binding energy. Open volume defects present in a sample, irrespective of their association with impurities could be detected by positron lifetime measurements. By means of TDPAC, the defects that are trapped by probe atoms are flagged by unique hyperfine interaction parameters. The defects associated with probe atoms can be identified unambiguously based on the correlation of the variation of hyperfine interaction parameters with annealing temperature with the results from other measurements such as resistivity and positron annihilation spectroscopy. Based on the commonalities and complementarities of TDPAC and positron lifetime techniques [16], combined measurements were done to address the problem of helium in *Zr*Hf.

The present work is aimed at studying the following by TDPAC and positron lifetime measurements in α-implanted *Zr*Hf sample: (1) to identify defects if any are trapped by (associated with) Hf impurities in the sample by TDPAC and their evolution with isochronal annealing treatment; (2) to study the helium implantation induced defects in the sample by positron lifetime measurements; (3) to find out the nucleation and growth stages of He bubbles in *Zr*Hf and also to find out the variation of bubble parameters such as radii and concentration with annealing temperature by positron lifetime measurements.

2. Experimental details

An alloy of Zr with 1 wt% Hf, each of 99.8% purity, has been prepared by arc melting in a helium atmosphere and homogenised by prolonged annealing. *Zr*Hf samples of 340 μm thickness were annealed at 1073 K at a pressure of 1.33×10^{-8} Pa for 3 h to obtain defect free reference samples. TDPAC measurement on the reference sample indicates that all probe nuclei experience a quadrupole frequency of 310 ± 4 MHz with an asymmetry parameter 0.07 ± 0.02. The fitted $R(t)$ spectrum and its Fourier transform are shown in Fig. 1. As the values of hyperfine interaction parameters coincides with that experienced by ^{181}Ta probe nuclei occupying defect free and substitutional sites in hcp Zr matrix [17], we infer that all the probe atoms are defect free and substitutional in Zr matrix.

These samples were homogeneously implanted with 40 MeV α-particles to a dose of 100 appm using a cyclotron at VECC, Calcutta. The temperature of the sample during irradiation was 323 ± 20 K. The α-particle beam passes through a rotating degrader wheel mounted with A1 foils of different thicknesses. This continuously degrades the beam energy resulting in a homogeneous helium distribution over the sample thickness [3]. The helium implanted and reference *Zr*Hf

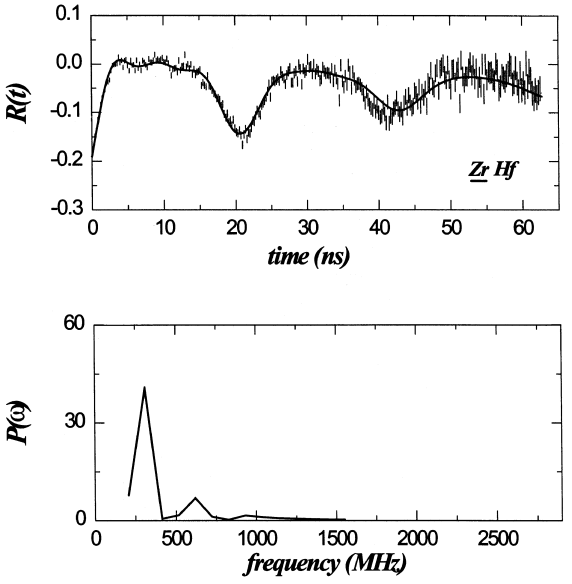

Fig. 1. (a) The experimental time dependent anisotropy spectra at room temperature in the reference α-*Zr*Hf sample. The continuous curve is the one calculated using the fitted values of the parameters. (b) The Fourier transform of the above spectra.

samples meant for TDPAC measurements were thermal neutron irradiated at the CIRCUS reactor at Bhabha Atomic Research Centre, Bombay, to a fluence of $2 \times 10^{22}\,\mathrm{n/m^2}$, to produce ^{181}Ta probe nuclei in the samples by the reaction $^{180}\mathrm{Hf}(\mathrm{n},\gamma)\,^{181}\mathrm{Hf} \rightarrow^{\beta^-}{}^{181}\mathrm{Ta}$.

The TDPAC of the 133–482 KeV $\gamma-\gamma$ cascade of ^{181}Ta was measured by a three detector twin fast–slow coincidence setup having NaI(T1) detectors. One of the detectors was gated for the START (133 keV) γ-ray, with respect to which the other two detectors were fixed at 90° and 180° for the detection of the STOP (482 keV) γ-ray. The time delayed coincidence spectra were obtained in the form of count rate as a function of the time elapsed after the emission of first γ-ray. The two time spectra $\mathrm{W}(90^\circ,t)$ and $\mathrm{W}(180^\circ,t)$ were recorded simultaneously. The prompt time resolution of the setup measured with a ^{60}Co source was 2.2 ns FWHM when gated for the above cascade of ^{181}Ta.

From the delayed coincidence spectra $\mathrm{W}(90^\circ,t)$ and $\mathrm{W}(180^\circ,t)$, the normalised anisotropy function $R(t)$ was calculated as

$$R(t) = A_2G_2(t) = 2 \times \frac{[W(180^\circ,t) - W(90^\circ,t)]}{[W(180^\circ,t) + 2W(90^\circ,t)]}, \qquad (1)$$

where A_2 is effective anisotropy coefficient and $G_2(t)$ is the perturbation factor. $W(90^\circ,t)$ and $W(180^\circ,t)$ are the coincidence count rates at 90° and 180°, respectively between the START and STOP detectors.

Therefore the $R(t)$ spectra were least squares fitted to the following function [7]:

$$R(t) = A_2G_2(t) = A_2\left[f_0 + f_1\sum_{m=0}^{3} a_m \exp[-\delta k_m(\eta)\omega_Q t]\cos[k_m(\eta)\omega_Q t]\right], \qquad (2)$$

where $k_0 = 0, k_1(\eta) + k_2(\eta) = k_3(\eta), \sum_{m=0}^{3} a_m(\eta) = 1$ and $f_0 + f_1 = 1$.

The spin value of the isomeric state of ^{181}Ta being $I = 5/2$ we have

$$v_Q = eQV_{zz}/h = 10\omega_Q/3\pi, \qquad (3)$$

where V_{zz} is the principal component of the electric field gradient (EFG) tensor. When the EFG is not axially symmetric, the asymmetry parameter $\eta = (V_{xx} - V_{yy})/V_{zz}$, where $|V_{zz}| \geqslant |V_{yy}| \geqslant |V_{xx}|$ is extracted from the fit of $R(t)$ data to Eq. (2). The values of k_m depend on η. Therefore the EFG tensor is completely determined by the frequency v_Q and the asymmetry parameter η. The exponential factor in the sum accounts for the possible existence of a quadrupole frequency distribution which is assumed to be correctly described by a Lorentzian shape with a relative width δ. A non-vanishing value of δ implies either a significant concentration of defects and/or impurities in the material under study, or with a disordered arrangement of atoms in the probe surroundings.

The positron lifetime measurements were carried out using fast-fast coincidence spectrometer with a time resolution (FWHM) of 220 ps. Lifetime spectra were analysed in terms of two components using POSITRONFIT [18] to obtain the resolved lifetimes and their intensities:

$$I(t) = I_1 \exp(-t/\tau_1) + I_2 \exp(-t/\tau_2), \qquad (4)$$

where τ_1 and τ_2 are the characteristic lifetimes and I_1 and I_2 the corresponding intensities. Here $I_1 + I_2 = 100\%$.

Positron lifetime and TDPAC measurements were done in the as-implanted state of the respective *Zr*Hf samples. Further measurements were carried out on the respective samples following isochronal annealing treatments of the samples from 323 K to 1373 K for a step duration of 30 min.

3. Results and discussion

TDPAC measurements on the reference sample indicate that all probe nuclei experience a quadrupole frequency of 310 ± 4 MHz with the other parameters viz., relative width of Lorentzian distribution and the asymmetry parameter being $\delta_1 = 0.08 \pm 0.03$ and $\eta_1 = 0.08 \pm 0.02$, respectively. The data analysed time dependent anisotropy spectrum and its Fourier transform are shown in Fig. 1. As the quadrupole frequency and other hyperfine interaction parameters match with

that of probe nuclei occupying defect free and substitutional sites in hcp Zr as reported in the literature [17], it is inferred that all probe nuclei occupy defect free and substitutional sites in the Zr matrix.

TDPAC measurements done on the helium implanted α-*Zr*HF samples have indicated the following hyperfine interaction parameters as experienced by probe atoms viz., $f_1 = 0.88 \pm 0.02$, $\nu_{Q1} = 310 \pm 4$ MHz, $\delta_1 = 0.14 \pm 0.03$ and $\eta_1 = 0.10 \pm 0.02$. Above results indicate that the fraction f_1 of probe nuclei occupies substitutional sites in hcp Zr matrix as mentioned above [17]. A low value of asymmetry parameter η in the above case implies an almost axially symmetric charge environment of probe nuclei. $R(t)$ spectra of the as-implanted sample indicates zero-offset (cf. Fig. 2(a)). Data analysis indicates that 0.12 fraction of probe nuclei is exposed to a zero quadrupole frequency. This configuration which removes the characteristic EFG of the hcp lattice must have cubic symmetry. This is possible by changing the hcp stacking sequence ABAB to ABCAB, thus generating a local fcc lattice with vanishing EFG and hence zero quadrupole frequency. A similar result in proton irradiated Cd has been reported by Witthuhn et al. using ^{111}Cd TDPAC measurements [19]. The probe associated defect cannot be a vacancy cluster, as the configuration of vacancy clusters bound to Hf impurity in a hcp matrix is not cubic. There is no significant increase in the value of the asymmetry parameter in the α-implanted sample as compared to that of the reference sample, implying almost an axially charge symmetric environment of the probe nuclei in the latter.

The measurement following the annealing treatment of the sample at 423 K indicates the disappearance of the zero-offset meaning the absence of the fraction f_0 appearing in Eq. (2). This implies the dissociation of the cubic symmetric defect complex from the probe nuclei. Further measurements following the isochronal annealing treatments of the sample did not lead to the appearance of any new quadrupole frequency. This is due to the non-trapping of helium implantation induced defects such as vacancy clusters and helium decorated vacancy complexes by probe nuclei. The non-trapping of vacancy type defects by Hf atoms is understandable considering the fact that both Hf and Zr are tetravalent with almost the same atomic radii. This observation is consistent with the earlier reported TDPAC measurements in quenched *Zr*Hf [20].

The variation of the relative width of the Lorentzian distribution δ_1 in the helium implanted *Zr*Hf with isochronal annealing temperature is shown if Fig. 3. This variation could be divided into three stages: In the annealing interval 300–500 K, the value of $\delta_1(0.14 \pm 0.04)$ remains nearly the same. In the annealing interval 500–950 K, δ_1 increases to a maximum around 850 K. Beyond 950 K, the δ_1 tends to decrease before levelling off. The striking feature seen in δ_1 between 500 and 800 K for the helium implanted sample, which is attributed to the recovery stage due to helium migration, is absent in the case of quenched *Zr*Hf [20]. The above variation of δ_1 with annealing temperature in

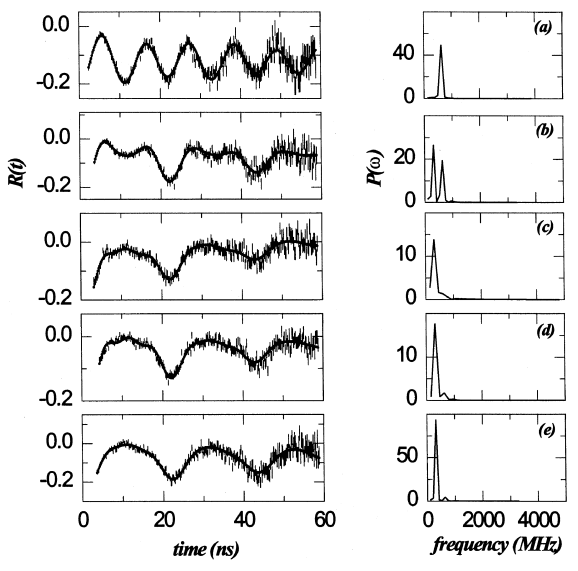

Fig. 2. The TDPAC spectra and their Fourier transform helium implanted α-*Zr*Hf sample subjected to following annealing treatments. (a) as-implanted (b) $T_a = 523$ K (c) $T_a = 873$ K (d) $T_a = 973$ K and (e) $T_a = 1123$ K.

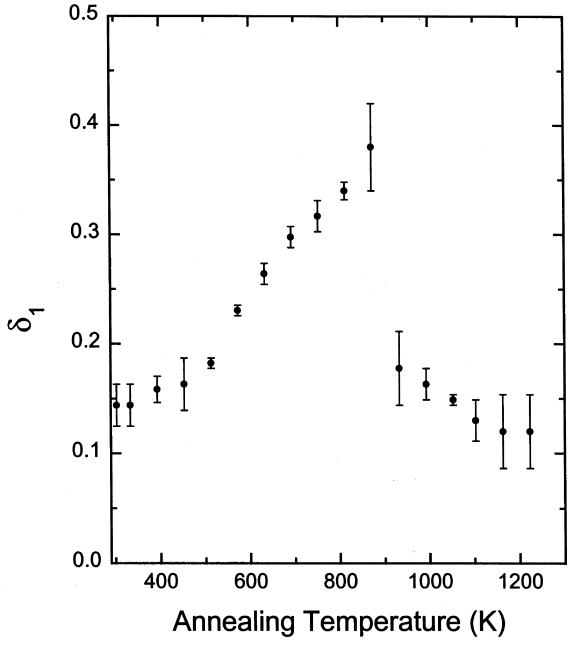

Fig. 3. The variation of δ_1 with annealing temperature of the sample.

helium implanted sample is understood based on the correlation of positron lifetime results as discussed subsequently.

The Fourier transform of the time dependent anisotropy spectra (Fig. 2) in the sample shows that the ratio of the intensities of the transition frequencies corresponding to ν_{Q1} is different from 3:2:1. This is due to texturing of the sample arising out of prior thermomechanical treatment. The location of the sample with its areal surface, lying perpendicular to the axis connecting START and STOP detectors which are at 180° with respect to each other, during the measurements is referred to as geometry I. The sample while located with its surface lying collinear to the above detectors during the measurements is referred to as geometry II. In Fig. 2 the $R(t)$ spectra corresponding to the as-implanted sample and isochronal annealing treatments at 423 K are due to the TDPAC measurements in geometry I and the remaining in geometry II.

Positron lifetime measurement on the reference ZrHf (un-implanted) sample indicates a single component with lifetime of 168 ± 2 ps which matches with that of α-*Zr* (165 ps) as reported earlier [21,22]. Positron lifetime measurements on the helium implanted sample indicate that 0.88 (I_1) fraction of positrons annihilates with a lifetime τ_1 of 225 ± 2 ps and the remaining with a lifetime (τ_2) of 480 ± 20 ps. As the lifetime of a positron at a monovacancy is reported to be 250 ± 5 ps [22] it is understandable that the observed lifetime of 225 ± 2 ps corresponds to He decorated vacancy in α-Zr [23]. Doppler broadening measurements on electron irradiated α-Zr [3] reveal that the onset of monovacancy migration occurs in the sample at 250 K. The formation of He–V complexes and vacancy clusters identified with τ_1 and τ_2 in the as-implanted sample is consistent with the above reported result.

The variation of resolved positron lifetime parameters with annealing temperature is shown in Fig. 4. Based on the variation of positron lifetime parameters with annealing temperature it is observed that the recovery of the defects in the He implanted sample occurs in three stages.

(i) In the annealing interval 300–523 K the values of τ_1, τ_2 and I_2 remain constant. This indicates the thermal stability of the He–V complexes and vacancy clusters.

(ii) For annealing interval between 523 and 673 K there occurs a sharp decrease in the values of τ_1 and τ_2 with annealing temperature. The value of τ_1 decreases from 220 to 120 ps, while τ_2 decreases from 480 to 260 ps. The value of I_2 reaches a maximum value at 673 K. The variation of intensity of the first component I_1 (i.e. $100 - I_2$) is opposite to that of I_2. The decrease in τ_1 between 500 and 700 K is understood to be due to the dissociation of He–V complexes. The dissociation of the He atoms from the He–V complexes and subsequent helium migration results in helium decoration of the vacancy clusters which is in accordance with the observed decrease in τ_2 to 260 ps. The temperature at which τ_2 exhibits a minimum and I_2 shows a maximum, is the onset of bubble nucleation. At this temperature the observed lifetime of $\tau_1 = 120$ ps is attributed to the bulkstate behaviour in accordance with the two state trapping model [12].

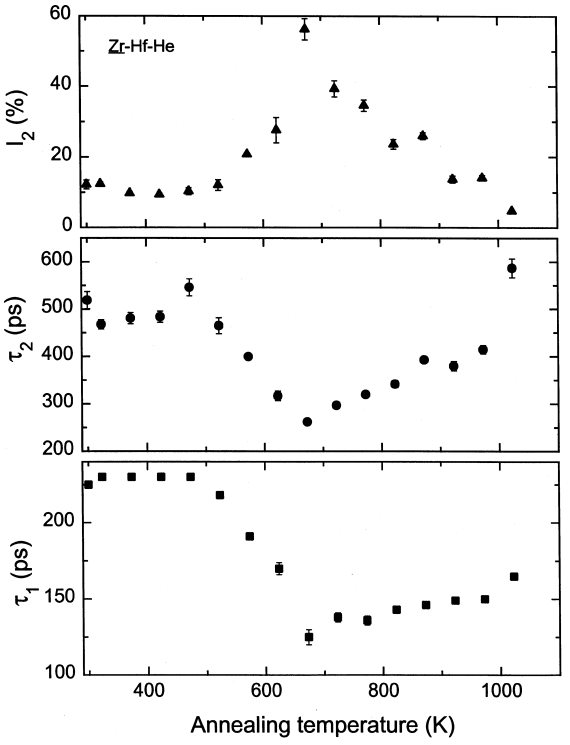

Fig. 4. Variation of resolved lifetime parameters with annealing temperature in helium implanted α-*Zr*Hf sample.

(iii) For annealing treatments above 673 K the value of I_2 decreases while τ_2 increases from an initial value of 260 ps. This indicates the growth of helium bubbles at the cost of the bubble concentration. The behaviour of I_2 at higher annealing temperature suggests that helium retention in bubbles is stable upto 1050 K.

Comparsion of TDPAC results as shown in Fig. 3 and positron lifetime results in Fig. 4 shows the following salient features for the helium implanted *Zr*Hf.

(1) The constant behaviour of the resolved positron lifetime parameters τ_1, τ_2 and I_2 in the annealing interval 300–500 K imply the stability of He-V complexes and vacancy clusters. The small vacancy clusters occupy the next nearest neighbouring environment sites of Hf impurities which is in accordance with the observed nearly constant behaviour of the relative width of the Lorentzian distribution of quadrupole frequency, δ_1.

(2) A decrease in τ_1 and τ_2 accompanied by an increase in I_2 between 500 and 800 K indicate dissociation

of He from He-V complexes and subsequent migration and decoration of vacancy clusters. These helium decorated defects provide a more non-unique next nearest neighbour environment at Hf sites resulting in the observed increase in δ_1 in the same annealing interval.

(3) Beyond 800 K, bubble growth is seen in the behaviour of positron lifetime parameters, where τ_2 increases towards saturation accompanied by a decrease in the intensity I_2. Since most of the vacancies and helium have been absorbed by the bubbles during growth, this leads to the restoration of nearly defect free environment of Hf site. The latter is in accordance with the observed sharp decrease in δ_1 in this annealing region as deduced by TDPAC. TDPAC measurements on the reference sample (un-implanted sample) subjected to the above annealing treatments did not show any variation in the hyperfine interaction parameters as experienced by probe nuclei. The maximum value of δ_1 occurring in the helium implanted sample around 870 K is consistent with the results based on nuclear reaction analysis, reported by Lewis et al. [24], who observed a significant broadening of helium profile in the same temperature range. The above discussions point to the merit of combining TDPAC and positron lifetime spectroscopy for the study of helium effects in metals.

4. Extraction of helium bubble parameters from positron lifetime results

The helium bubble parameters such as helium atom density (n_{He}) inside the bubble, bubble radius (R_b) and bubble concentration (C_b) have been determined from an analysis of experimental positron lifetime results based on the procedure reported earlier [3]. We briefly summarise below the analysis scheme used. Based on the positron surface state model [25], the most stable positron state is at the surface of the bubble of radii > 0.5 nm. Considering the gas–metal interface, positrons will be annihilating with electrons associated with both the metal and helium. As these two annihilation processes are independent the total annihilation rate can be written as

$$\lambda_{bubble} = \lambda_{He} + \lambda_{metal}. \tag{5}$$

λ_{metal} is characteristic of the annihilation rate for clean metal surface. This is almost same for most of the metals having a value of $\approx 2\,ns^{-1}$. λ_{He} depends on the helium atom density n_{He}. The relationship connecting bubble lifetime τ_2 and helium atom density n_{He} is given by [25]

$$\tau_2 = 500 - 23.5 n_{He}(10^{28} m^{-3}). \tag{6}$$

Although the above equation was originally proposed for the Al–He system it can be applied as a first approximation for most metal–He systems [13,25]. Using τ_2 in the above equation, n_{He} can be determined. On the basis of two state trapping model [11], the trapping rate, K_b, into the bubbles can be deduced from the measured lifetime parameters as

$$K_b = I_2(\lambda_1 - \lambda_2), \tag{7}$$

where λ_1 and λ_2 are experimental annihilation rates in the bulk and bubble, respectively and I_2 is the intensity of the bubble lifetime component. The trapping rate K_b can be related to bubble concentration, C_b, as

$$K_b = \mu_b C_b, \tag{8}$$

where μ_b is the specific trapping rate of positrons to the bubble. The size dependence of μ_b is taken into account by using a semi-empirical relation for μ_b, given by [3]

$$\mu_b = \left[\frac{1}{AR_b} + \frac{1}{BR_b^2}\right]^{-1}, \tag{9}$$

where the constants are given by $A = 9.07 \times 10^{16}\,nm^{-1}\,s^{-1}$ and $B = 3.3 \times 10^{16}\,nm^{-2}\,s^{-1}$. If the total gas concentration, C_{He}, implanted into the sample is known and all the gas is assumed to be contained in spherical bubbles, then the helium inventory equation can be written as

$$C_{He} = \frac{4\pi R_b^3 n_{He} C_b}{3}. \tag{10}$$

The above assumption that all the input helium is contained in the bubbles is justified because of the fact that samples of thickness greater than 100 μm are used for PAS and helium loss from the bubble to the sample surface is expected to be negligible.

Using the Eqs. (7)–(10), an equation for R_b can be written as

$$BR_b^2 + AR_b - 3AB\left(\frac{C_{He}}{4\pi I_2(\lambda_1 - \lambda_2) n_{He}}\right) = 0. \tag{11}$$

With n_{He} known from Eq. (6) and with the known value of C_{He}, the above equation is solved for R_b. Once R_b is known, the bubble concentration C_b can be obtained using Eq. (10).

The variation of R_b and C_b, as deduced from the above discussed analysis scheme are shown in Fig. 5(a) and (b). R_b increases from a value of 4 nm at 700 K to 15 nm at 1000 K, while C_b decreases by an order of magnitude in the same annealing interval. This establishes quantitatively the helium bubble growth.

5. Conclusions

TDPAC measurements on the helium implanted *Zr*Hf indicate the formation of stacking fault kind of defects, which is consistent with the low value of the stacking fault energy reported in literature for hcp metals in general. These defects dissociate above 423 K.

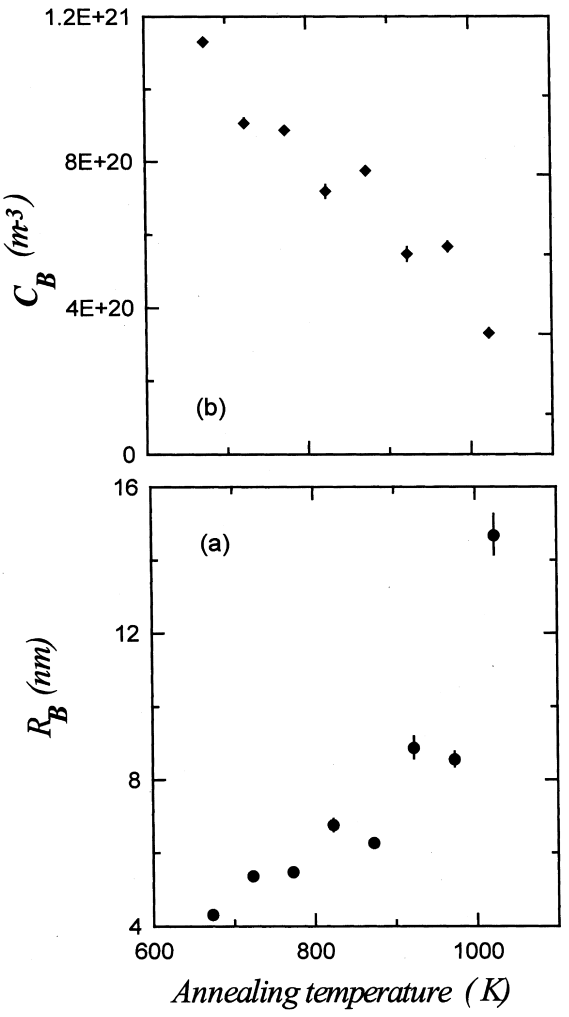

Fig. 5. Variation of (a) bubble radius and (b) bubble concentration with annealing temperature in the helium implanted α-*Zr*Hf as deduced from the positron lifetime results.

A good correlation of a recovery stage above 500 K associated with helium migration is seen from the variation of the relative width of the Lorentzian distribution of the quadrupole frequency as experienced by the Hf probe atom in comparison to the variation of the positron lifetime in the helium implanted *Zr*Hf. Nucleation and growth of helium bubbles have been identified from positron lifetime results. The onset of growth of He bubbles occurs at 673 K. Helium bubble parameters in the growth stage have been extracted from an analysis of the results of positron lifetime measurements. Since Hf impurities do not bind vacancy type defects in Zr, it seems unlikely that Hf mediated He-vacancy interactions influence the bubble formation. The present study points to the merit of combining TDPAC and positron lifetime spectroscopy for the study of helium effects in metals.

Acknowledgements

We thank Dr Amarendra and Dr R. Rajaraman for their help during the irradiation experiments. Useful discussions with Dr C.S. Sundar are gratefully acknowledged.

References

[1] H. Ullmaier, Radiat. Eff. 78 (1983) 1.
[2] W.D. Wilson, C.L. Bisson, M.I. Bakes, Phys. Rev. B 24 (1981) 5616.
[3] G. Amarendra, B. Viswanathan, A. Bharathi, K.P. Gopinathan, Phys. Rev. B 45 (1992) 10231.
[4] A. Van Veen, Mater. Sci. Forum. 15&16 (1987) 3.
[5] C.D. Van Siclen, R.N. Wright, Phys. Rev. Lett. 26 (1992) 3892.
[6] G. Amarendra, B. Viswanathan, R. Rajaraman, S. Srinivasan, K.P. Gopinathan, Philos. Mag. Lett. 65 (1992) 77.
[7] E. Recknagel, G. Schatz, Th. Wichert, in: J. Christiansen (Ed.), Hyperfine Interactions of radioactive nuclei, Springer, Heidelberg, 1983.
[8] G.S. Collins, S.L. Shropshire, J. Fan, Hyp. Int. 62 (1990) 1.
[9] Th. Wichert, Radiat. Eff. 78 (1993) 177.
[10] L. Niesen, Hyp. Int. 10 (1981) 619.
[11] P. Hautojarvi (Ed.), Positrons in Solids, Springer, Berlin, 1979.
[12] W. Brandt, A. Dupasquier (Eds.), Positron Solid State Physics, North-Holland, Amsterdam, 1983.
[13] K.O. Jensen, Fundamental Aspects of Inert Gases in Solids, S.E. Donnelly, J.H. Evans (Eds.), Plenum, New York, 1990, p. 195.
[14] Positron Annihilation Studies in Materials Science, in: B. Viswanathan, C.S. Sundar (Eds.), Metals, Materials and Processes vol. 8, 1996.
[15] G.M. Hood, J. Nucl. Mater. 159 (1988) 149.
[16] Th. Wichert, Mater. Sci. Forum. 15&16 (1987) 829.
[17] R. Vianden, Hyp. Int. 15&16 (1983) 1081.
[18] P. Kirkegaard, M. Eldrup, O.E. Mogensen, N.J. Pedersen, Comp. Phys. Commun. 23 (1981) 307.
[19] W. Witthuhn, A. Weidinger, W. Sandner, H. Metzner, W. Klinger, R. Bohm, Z. Phy. B 33 (1979) 155.
[20] R. Govindaraj, K.P. Gopinathan, J. Nucl. Mater. 231 (1996) 141.
[21] A. Seeger, F. Banhart, W. Bauer, in: L. Dorikens-Vanpraet, M. Dorikens, D. Segers (Eds.), Positron Annihilation, World Scientific, Singapore, 1989, p. 275.
[22] T. Gorecki, Mater. Sci. Forum. 105–110 (1992) 643.
[23] G. Venugopal Rao, R. Govindaraj, K.P. Gopinathan, B. Viswanathan, Solid State Physics (India). 39C (1996) 199.
[24] M.B. Lewis, K. Farrell, Nucl. Inst. and Meth. B 16 (1986) 163.
[25] K.O. Jensen, R.M. Nieminen, Phys. Rev. B 35 (1987) 2087.